Electronic Supplementary Material (ESI) for ChemComm.

Supporting information

Direct thermolysis of CO_2 into CO and O_2

Qingqing Jiang,[a] Zhenpan Chen,[a], [b] Jinhui Tong,[a] Min Yang,[a] Zongxuan Jiang,[a] and Can Li [a] *

[a] State Key Laboratory of Catalysis, Dalian Institute of Chemical Physics, Chinese Academy of Sciences, Dalian National Laboratory for Clean Energy, Dalian, Liaoning 116023, R.P. China

[b] University of the Chinese Academy of Sciences, Beijing 100049, China

* To whom correspondence should be addressed. Email: canli@dicp.ac.cn

Tel: (+86) 411-84379070, Fax: (+86) 411-84694447

Experimental details

Samples preparation

All chemical reagents were analytical grade and were used as purchased without further purification. The commercial CeO_2, SiO_2 and ZrO_2 samples are used directly. The $Ce_{0.75}Zr_{0.25}O_2$, $LaFeO_3$, $LaFe_{0.7}Co_{0.3}O_3$ and $LaFe_{0.95}Pt_{0.05}O_3$ samples were prepared by a single step solution combustion method. In a typical preparation procedure, stoichiometric of raw materials ($Ce(NO_3)_3 \cdot 6H_2O$, $Zr(NO_3)_4 \cdot 5H_2O$, $La(NO_3)_3 \cdot 6H_2O$, $Fe(NO_3)_3 \cdot 9H_2O$, $Co(NO_3)_2 \cdot 6H_2O$, H_2PtCl_6 and glycine) were dissolved in a minimum volume of water and then it was transferred to furnace kept at 500 ^oC. Then, the sample was calcined at 800 ^oC for 4 h. The preparation of other samples followed the similar procedure. The phase compositions of synthesized oxides were confirmed by PXRD (Figure S4).

Characterization of samples

The synthesized samples were characterized by X-ray powder diffraction (XRD) on a Rigaku D/Max-2500/PC powder diffractometer. Each powder sample was scanned using Cu Kα radiation with an operating voltage of 40 kV and an operating current of 200 mA. The XRD patterns are recorded in the range of 20 - 80 ° with a scan rate of 5 ° min^{-1} and a step size of 0.02 °. The specific surface areas of these samples were determined with a Micromeritics ASAP 2000 adsorption analyzer. The morphologies and particle sizes were examined by scanning electron microscopy (SEM) with a Quanta 200 FEG scanning electron microscope.

CO_2-splitting test

The direct thermolysis of CO_2 was carried out in a vertical alumina tubular reactor (Al_2O_3 purity 99%), which was placed inside an electric furnace. In a general experiment, 0.5 g of metal oxide was loaded into the alumina tubular reactor via an internal corundum crucible. The argon (purity 99.9996%) and CO_2 (purity 99.999%) were passed through a de-oxidation tube to get rid of the residual O_2 before it passed into the reactor. Before the CO_2-splitting test, the argon (500 mL min^{-1}) was firstly passed

through the reactor and the electric furnace was pre-heated to a given temperatures (1100 - 1450 ^{o}C) with a ramping rate of 20 ^{o}C min^{-1}; then CO_2 (purity 99.999%) with a flow rate of 500 mL min^{-1} was injected into the reactor. The O_2 gas was analyzed by a gas chromatograph (Aligent 6890) equipped with a 5Å molecular sieve column and a TCD detector; the CO gas product was analyzed by a gas chromatograph (Aligent 6890) equipped with a GDX-102 column, a nickel conversion furnace and a FID detector. The outlet gases were analyzed by a frequency of ca. 2 min. All products were calibrated with standard known concentration gases.

1. Thermodynamic calculation for direct CO_2-splitting reaction at 1 bar

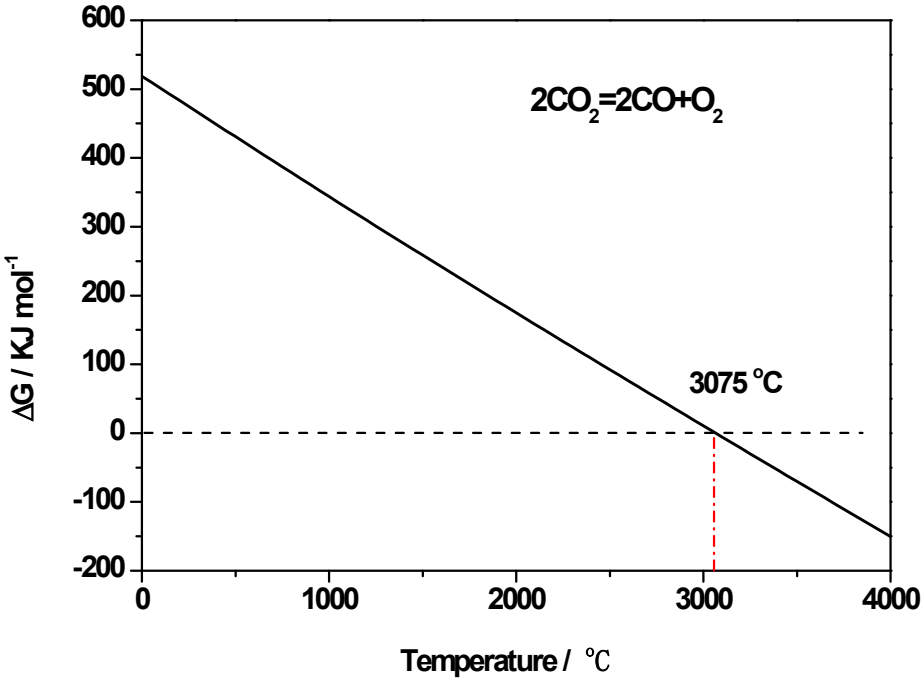

Figure S1. Temperature variations of ΔG for direct thermal CO_2-splitting at 1 bar.

Table S1. Temperature variations of ΔH, ΔG, ΔS and K for direct thermal CO_2-splitting at 1 bar

Temperature / °C	ΔH / KJ mol^{-1}	ΔS / J mol^{-1}	ΔG / KJ mol^{-1}	K [a]	Conversion / ‰
900	563.8	172.8	361.1	8.33E-17	0.004
1000	562.9	172.1	343.9	7.78E-15	0.02
1100	562.0	171.4	326.7	3.73E-13	0.07
1200	561.0	170.7	309.6	1.05E-11	0.22
1300	560.0	170.0	292.5	1.93E-10	0.58
1400	559.0	169.4	275.6	2.49E-09	1.35
1500	558.0	168.8	258.7	2.40E-08	2.88
1600	557.0	168.3	241.8	1.80E-07	5.63

[a] Reaction equation: $2CO_2 = 2CO + O_2$.

2. Schematic of testing system for direct thermochemical CO_2-splitting reaction

The outer diameter and inner diameter of the alumina tubular reactor is 21 mm and 14 mm, respectively.

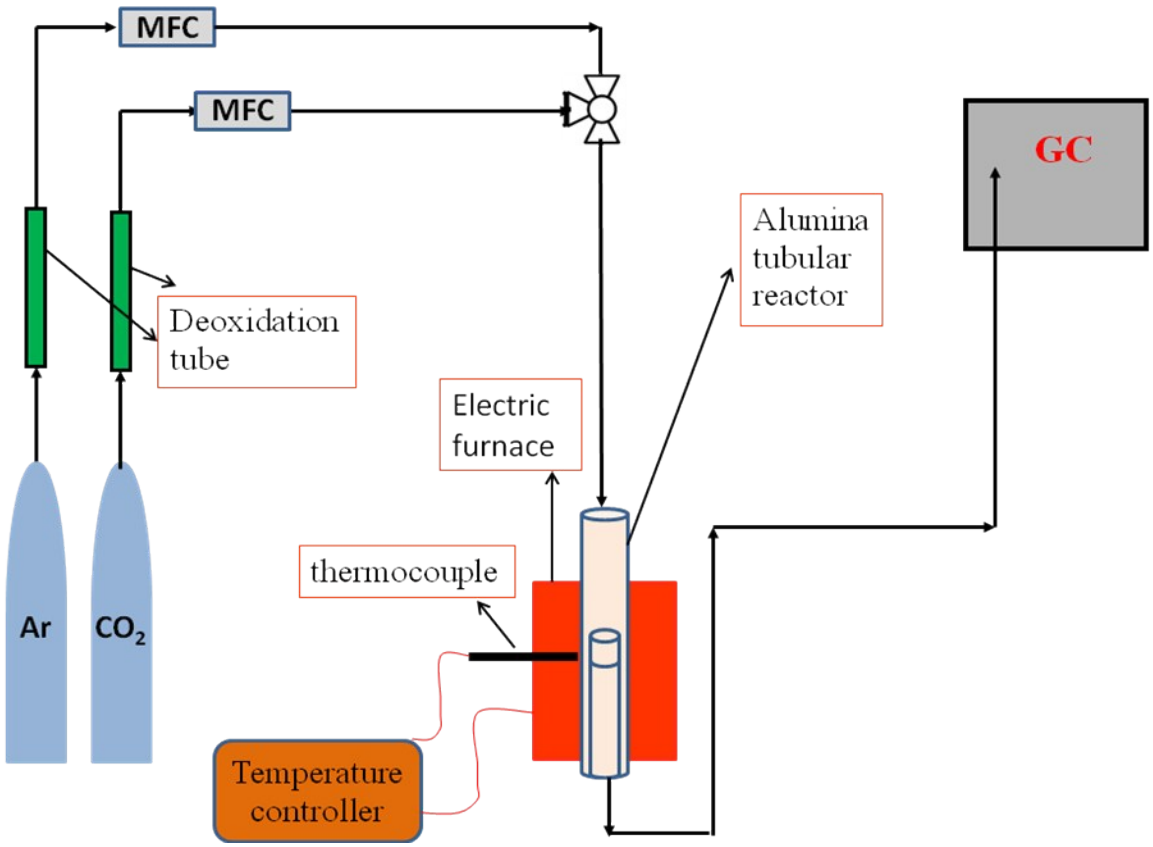

Figure S2. Schematic of testing system for direct thermochemical CO_2-splitting reaction.

3. GC signals of direct thermochemical CO_2-splitting

The O_2 gas was analyzed by a gas chromatograph (Aligent 6890) equipped with a 5Å molecular sieve column and a TCD detector. The CO gas product was analyzed by a gas chromatograph (Aligent 6890) equipped with a GDX-102 column and a FID detector. The outlet gas composition was detected every ca. 2 min.

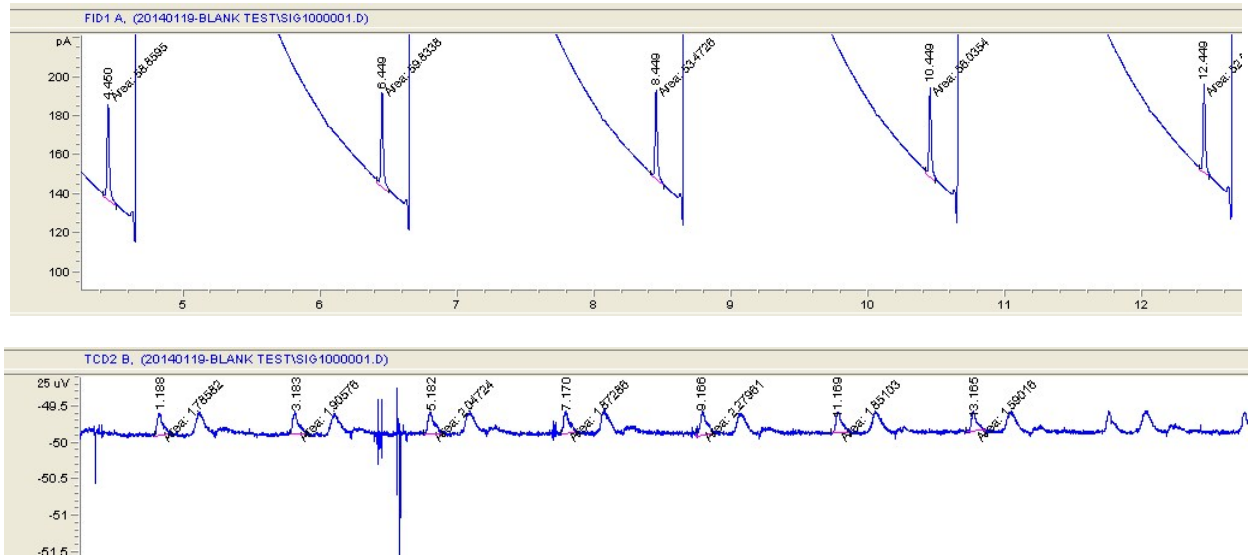

Figure S3(a). The GC signals of CO and O_2 for blank test at 1200 °C.

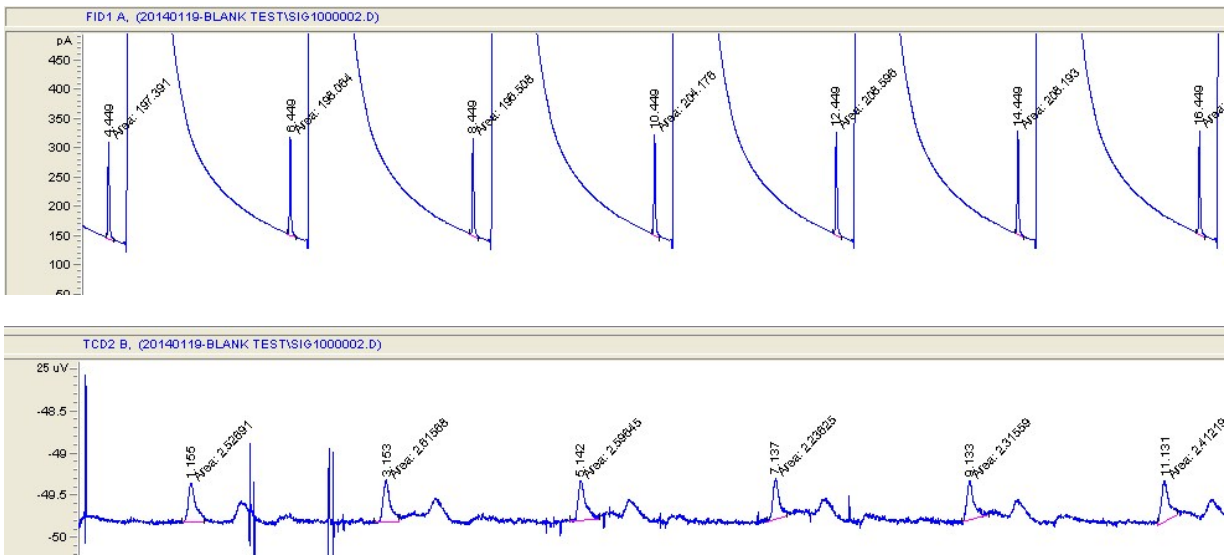

Figure S3(b). The GC signals of CO and O_2 for blank test at 1300 °C.

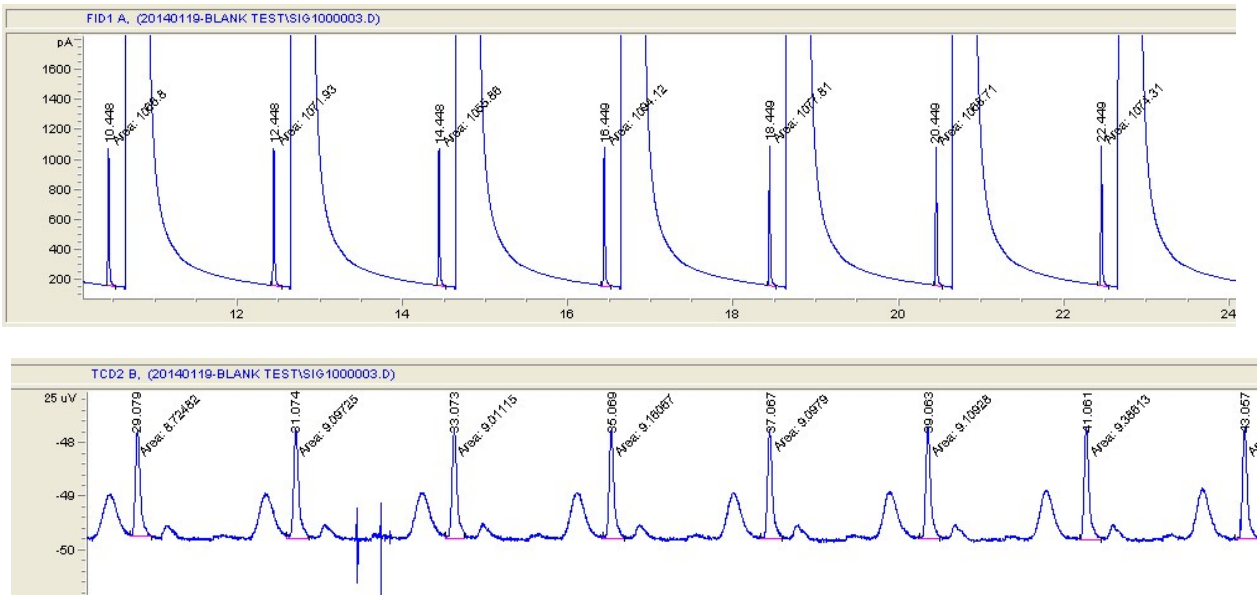

Figure S3(c). The GC signals of CO and O_2 for blank test at 1400 ^{o}C.

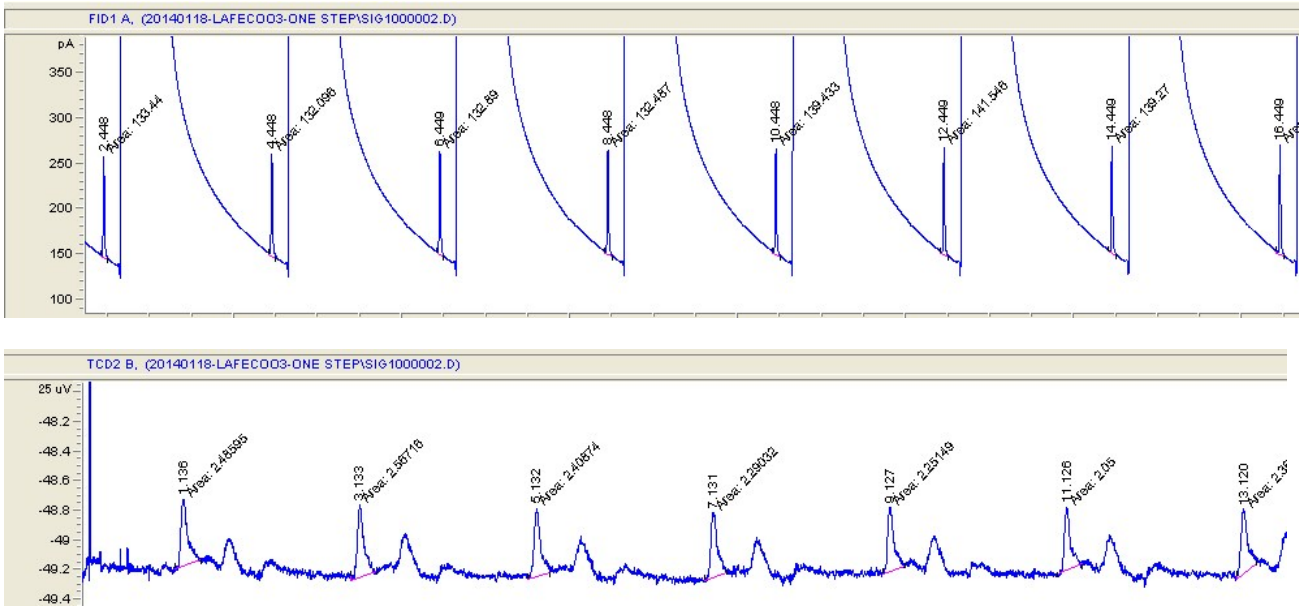

Figure S3(d). The GC signals of CO and O_2 for $LaFe_{0.7}Co_{0.3}O_3$ (0.5 g) at 1200 ^{o}C.

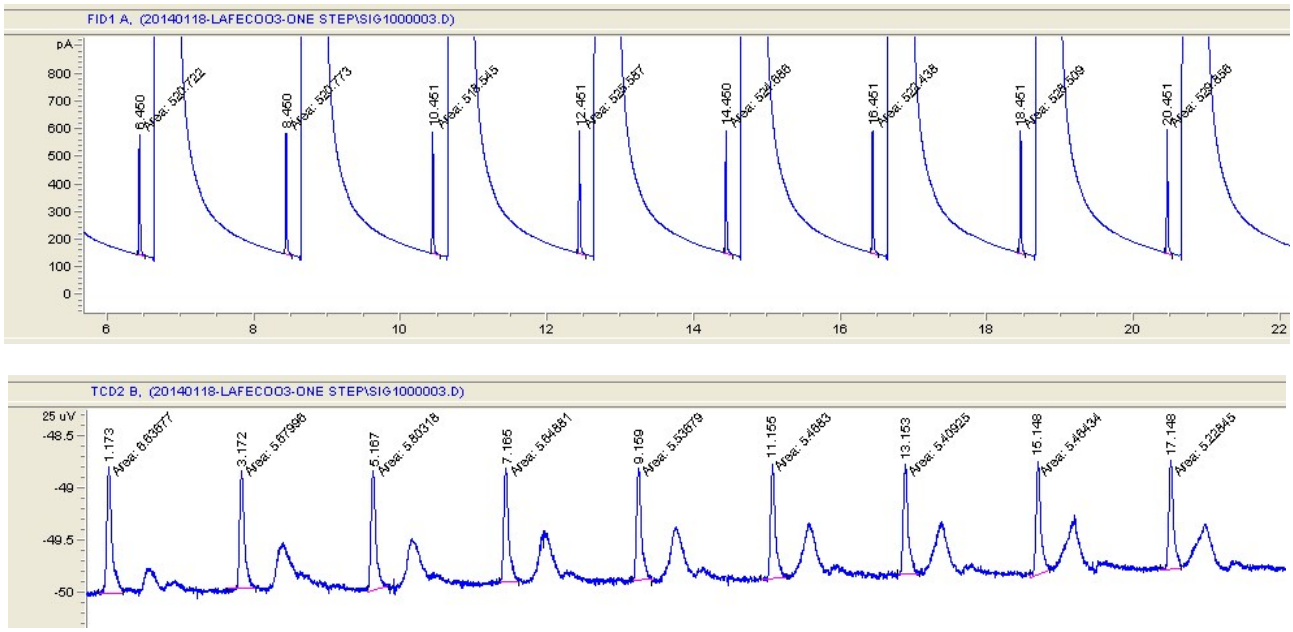

Figure S3(e). The GC signals of CO and O_2 for $LaFe_{0.7}Co_{0.3}O_3$ (0.5 g) at 1300 °C.

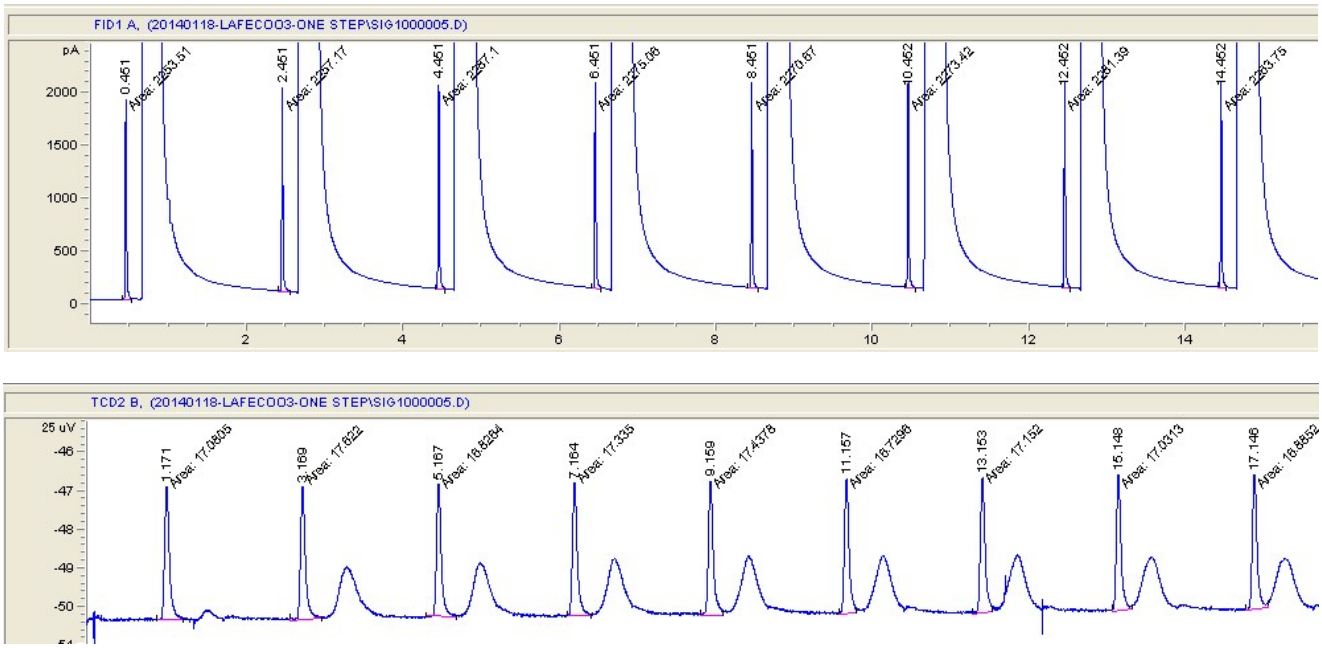

Figure S3(f). The GC signals of CO and O_2 for $LaFe_{0.7}Co_{0.3}O_3$ (0.5 g) at 1400 °C.

4. Physicochemical properties of oxides before and after the reaction

The BET surface areas, PXRD patterns and SEM images of different metal oxides are shown in Table S2, Figure S4 and Figure S5, respectively. It can be seen from Figure S4 that the synthesized $Ce_{1-x}Zr_xO_2$ samples adopt a typical fluorite structure and the $LaFe_{1-x}Co_xO_3$ samples adopt orthorhombic perovskite-type structure.

Table S2 BET surface areas of different metal oxides before and after the reaction

Samples	Specific surface area / $m^2\ g^{-1}$	
	before reaction	after reaction
ZrO_2	6.2	0.7
SiO_2	1.5	0.8
CeO_2	6.6	2.3
$Ce_{0.75}Zr_{0.25}O_2$	44.0	2.5
$LaFeO_3$	15.9	0.2
$LaFe_{0.7}Co_{0.3}O_3$	1.9	0.3

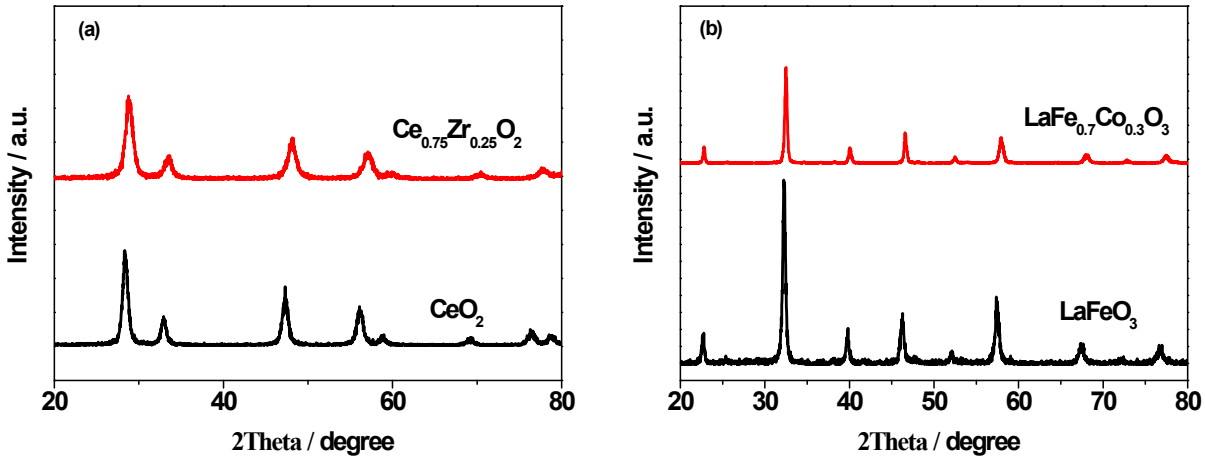

Figure S4. XRD patterns of (a) CeO_2 and $Ce_{0.75}Zr_{0.25}O_2$; (b) $LaFeO_3$ and $LaFe_{0.7}Co_{0.3}O_3$.

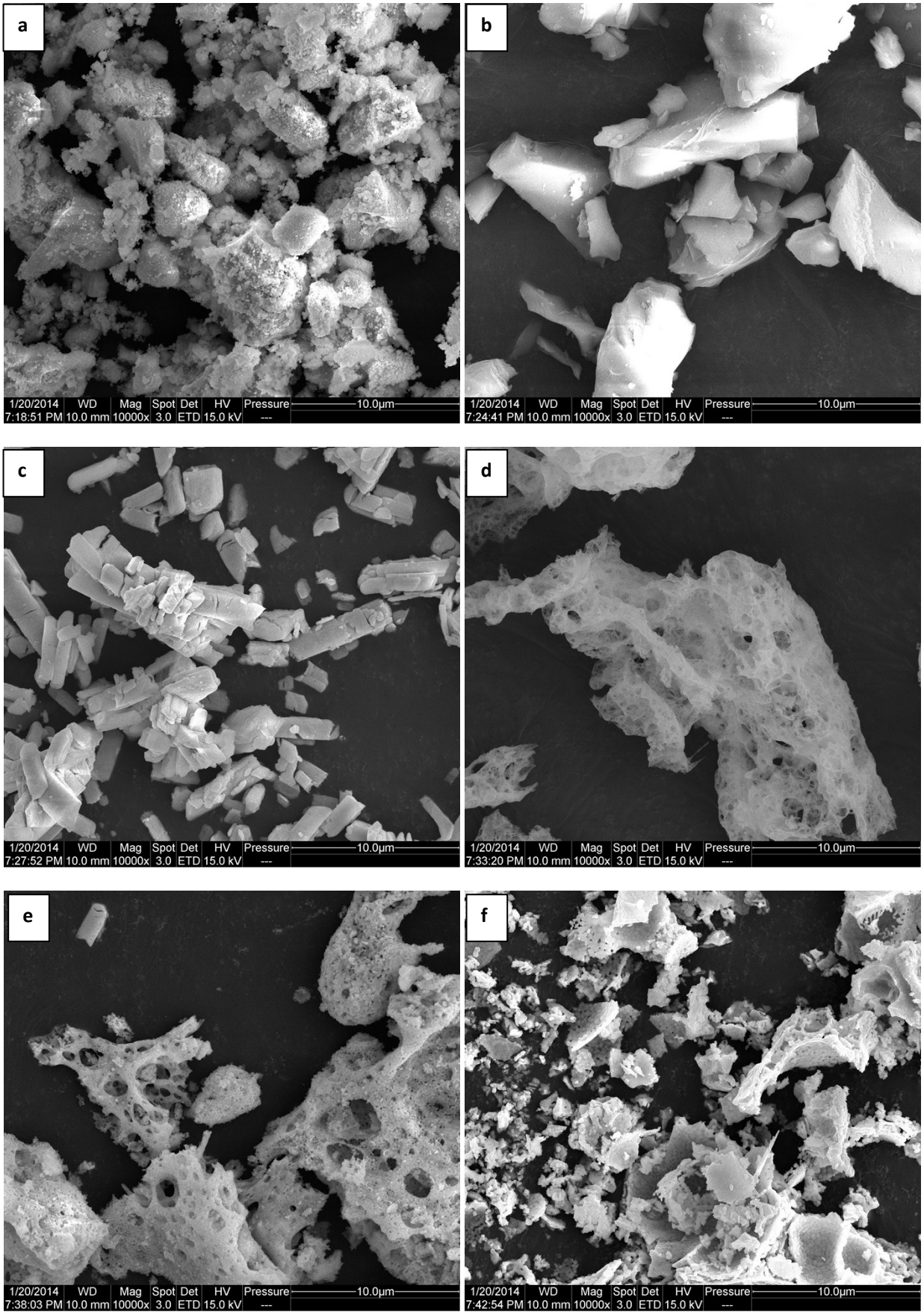
a
1/20/2014 WD Mag Spot Det HV Pressure 10.0µm
7:18:51 PM 10.0 mm 10000x 3.0 ETD 15.0 kV ---
b
1/20/2014 WD Mag Spot Det HV Pressure 10.0µm
7:24:41 PM 10.0 mm 10000x 3.0 ETD 15.0 kV ---
c
1/20/2014 WD Mag Spot Det HV Pressure 10.0µm
7:27:52 PM 10.0 mm 10000x 3.0 ETD 15.0 kV ---
d
1/20/2014 WD Mag Spot Det HV Pressure 10.0µm
7:33:20 PM 10.0 mm 10000x 3.0 ETD 15.0 kV ---
e
1/20/2014 WD Mag Spot Det HV Pressure 10.0µm
7:38:03 PM 10.0 mm 10000x 3.0 ETD 15.0 kV ---
f
1/20/2014 WD Mag Spot Det HV Pressure 10.0µm
7:42:54 PM 10.0 mm 10000x 3.0 ETD 15.0 kV ---

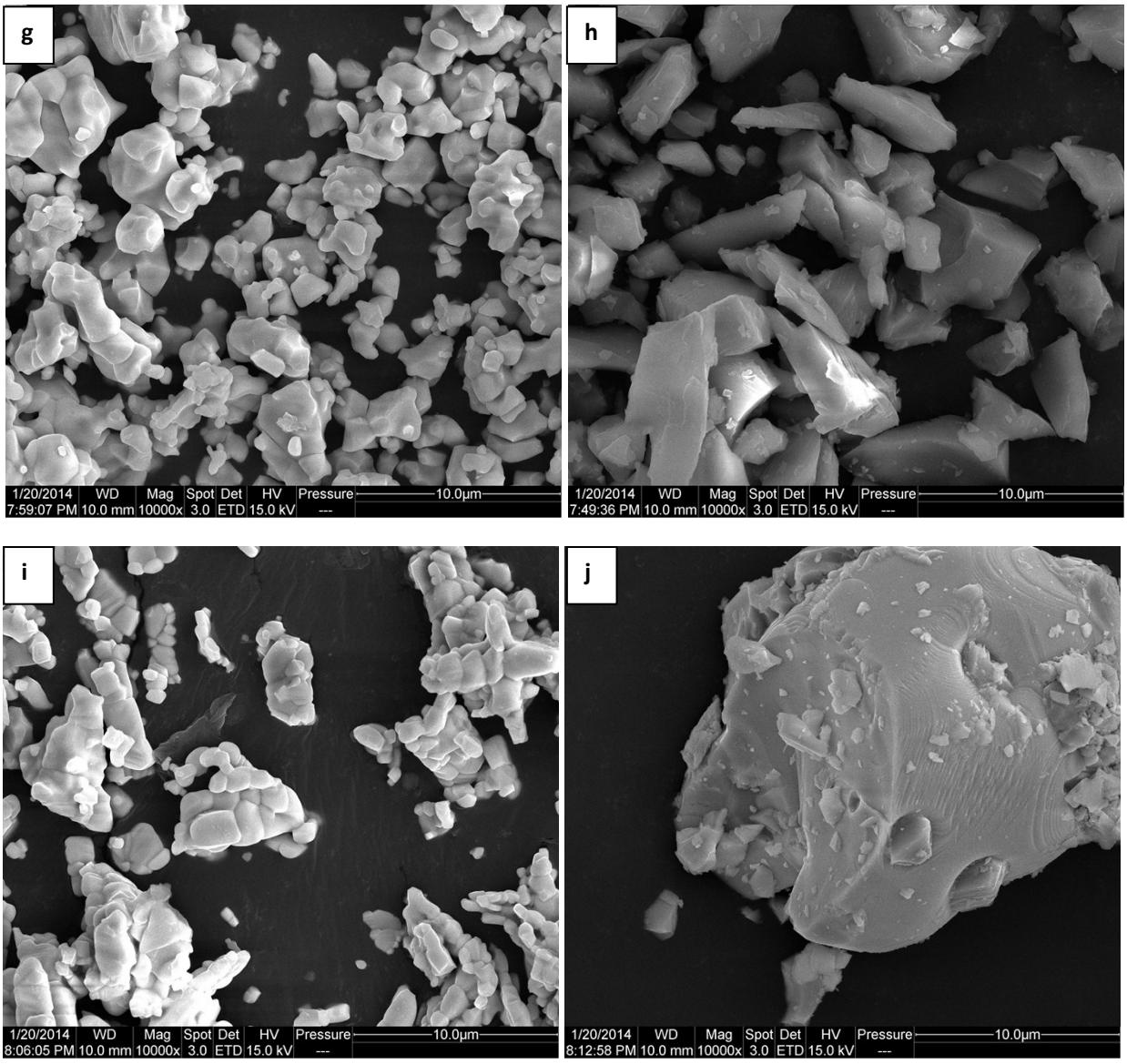

Figure S5. SEM images of (a) ZrO_2, (b) SiO_2, (c) CeO_2, (d) $Ce_{0.75}Zr_{0.25}O_2$, (e) $LaFeO_3$, (f) $LaFe_{0.7}Co_{0.3}O_3$, (g) ZrO_2 - after reaction at 1400 ^oC, (h) SiO_2 - after reaction at 1400 ^oC, (i) CeO_2 - after reaction at 1400 ^oC, (j) $LaFe_{0.7}Co_{0.3}O_3$ - after reaction at 1400 ^oC.

5. The possible mechanism for inert oxides (SiO_2, ZrO_2) and the blank tube

For inert oxides (SiO_2, ZrO_2) and the blank tube, the possible mechanism is shown in Figure S6. Generally, three reversible basic elementary reactions are assumed to take place under high temperatures. Firstly, the CO_2 molecule collided with the solid metal oxides walls (M), which initiates decomposition of CO_2 to CO and O atom; then CO_2 gas molecule is possible to contact with O atom which generates CO and O_2 molecules. The O_2 molecule is also possible to split into two O atoms through collisions with the surface. The presence of ZrO_2 and SiO_2 provide more site for the collide process. Besides, a small amount of oxygen vacancies also could be produced on the surface of the insert oxides at high temperatures.

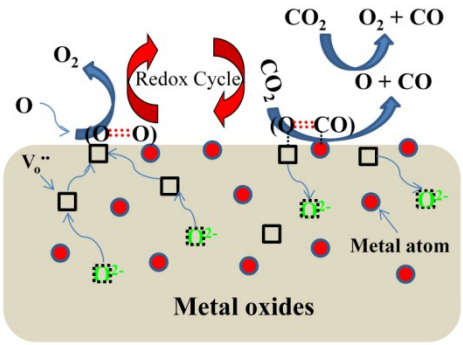

Figure S6. Possible reaction mechanism for direct CO_2 splitting reaction in the presence of ZrO_2 and SiO_2

6. Elementary reactions of direct thermolysis of CO_2 under high temperatures

Thermodynamically, it is feasible to dissociate CO_2 at high temperatures. The possible catalytic process of metal oxides enhanced direct thermolysis of CO_2 is illustrated in Figure 5. Generally, three reversible basic elementary reactions (eq. S1-3)[1] are assumed to take place for the direct thermochemical CO_2-splitting under high temperatures, where M represents a solid wall. Herein, eq. S1 represents the collision of CO_2 and solid metal oxides walls (M), which initiates the decomposition of CO_2; then the CO_2 gas molecule is possible to contact with O atom which generates CO and O_2 molecules (eq. S2). Also, the O_2 molecule is possible to split into two O atoms through collisions (eq. S3). Furthermore, in some cases, isothermal redox cycle of redox metal oxides (such as $Ce_{1-x}Zr_xO_2$, $LaFe_{1-x}Co_xO_3$) can take place simultaneously during this high temperature CO_2-splitting process (eq. S4). The corresponding reaction rate constants of eq. S1-S3 have been previously modeled by Tsang, W. and Hampson, R. F. with an extended Arrhenius expression (eq. S5), see details in Table S3.[1c, 2] Although this high temperatures dissociation process is followed by severe CO recombination reaction, it is possible to obtain the splitting CO and O_2 products via rapid cooling method.

Eq. S1-S4:

$$CO_2 + M \overset{R1}{\underset{R2}{\rightleftharpoons}} CO + O + M \qquad (S1)$$

$$CO_2 + O \overset{R3}{\underset{R4}{\rightleftharpoons}} CO + O_2 \qquad (S2)$$

$$O_2 + M \overset{R5}{\underset{R6}{\rightleftharpoons}} O + O + M \qquad (S3)$$

$$MO_x \overset{+\delta O_2}{\underset{-O_2}{\rightleftharpoons}} MO_{x-\delta} \qquad (S4)$$

$$k = AT^b \exp(-Ea / RT) \qquad (S5)$$

Table S3 The estimated kinetic parameters for the six reactions[1c, 2]

Reactions	Pre-exponential factor (A)	b	Activation energy (Ea/R)
R1	6.445×10^{10} m^3 mol^{-1} s^{-1}	0	62 600 K
R2	6.167×10^{2} m^6 mol^{-2} s^{-1}	0	1 510 K
R3	1.686×10^{7} m^3 mol^{-1} s^{-1}	0	26 500 K
R4	2.530×10^{6} m^3 mol^{-1} s^{-1}	0	24 000 K
R5	1.807×10^{12} m^3 mol^{-1} s^{-1}	−1	59 380 K
R6	1.886×10^{1} m^6 mol^{-2} s^{-1}	0	−900 K

7. Raman spectrum for CeO_2 and $Ce_{0.75}Zr_{0.25}O_2$ before and after high temperature reaction

Fig. S7(a) shows the Raman spectrum with excitation laser line at 325 nm for CeO_2 and $Ce_{0.75}Zr_{0.25}O_2$. The band at ca. 600 cm^{-1} is ascribed to the intrinsic oxygen vacancies and the relative ratio of band intensities between 600 cm^{-1} and 465 cm^{-1} has been related to the concentration of oxygen vacancies, and the higher the I_{600}/I_{465} ratio, the higher the concentration of oxygen vacancies. Fig. 7 (a) indicates that $Ce_{0.75}Zr_{0.25}O_2$ contains more oxygen vacancies than CeO_2. Fig. 7 (b) shows the Raman spectrum with excitation laser line at 532 nm for CeO_2 and $Ce_{0.75}Zr_{0.25}O_2$ after high temperature reaction. A certain amount of oxygen vacancies are still present for $Ce_{0.75}Zr_{0.25}O_2$ after high temperature reaction.

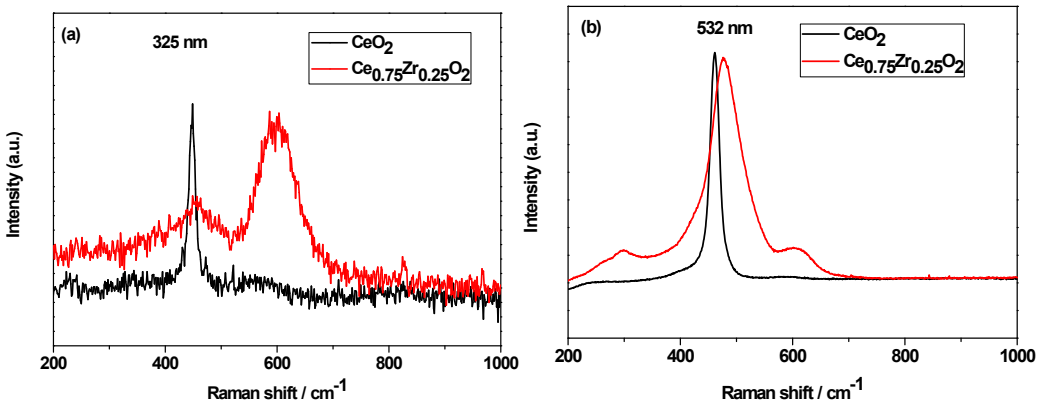

Figure S7. Raman spectra of (a) the as prepared CeO_2 and $Ce_{0.75}Zr_{0.25}O_2$ at 325 nm (b) the CeO_2 and $Ce_{0.75}Zr_{0.25}O_2$ samples after high temperature reactions at 532 nm

8. The CO generation rate as a function of CO_2 flow rate

The CO generation rate as a function of different CO_2 flow rate at 1300 °C in direct CO_2 decomposition reaction is shown in Figure S7. The CO generation rate increases as the increasing of CO_2 flow rate. Notably, the conversion ratio of CO_2 gradually increases as the increasing of CO_2 flow rate and reaches a maximal value of ~0.2 ‰ when the CO_2 flow rate is 500 mL min^{-1}. Without the addition of metal oxides, the CO_2 conversion is much lower (0.057 ‰) than that of $LaFeO_3$ (0.079 ‰), $LaFe_{0.7}Co_{0.3}O_3$ (0.149 ‰) and $LaFe_{0.95}Pt_{0.05}O_3$ (0.204 ‰), under the same experimental conditions (Figure S6b). It is interesting that the catalytic performance of metal oxide can be modulated by the design of compositions; when a small amount of PtO_x (5 atom %) is doped into the structure of $LaFeO_3$, the CO_2 conversion can be increased by 1.5-fold. This catalytic function of PtO_x is similar to our previous study on IrO_x catalyzed CO_2 splitting under high temperatures.[3] It should be stated that the thermodynamically calculated conversion of CO_2 is ~0.58 ‰ at 1300 °C (see Table S1). Actually, the theoretical CO_2 conversion ratio should be higher than that of ~0.58 ‰ since the reactor used here is an open system rather than a closed system. Herein, the actual conversion is lower than that of the theoretical value, which indicates that the reaction kinetics is the control step for CO_2-splitting at high temperatures and the presence of metal oxides act as a catalyst to enhance the kinetics.

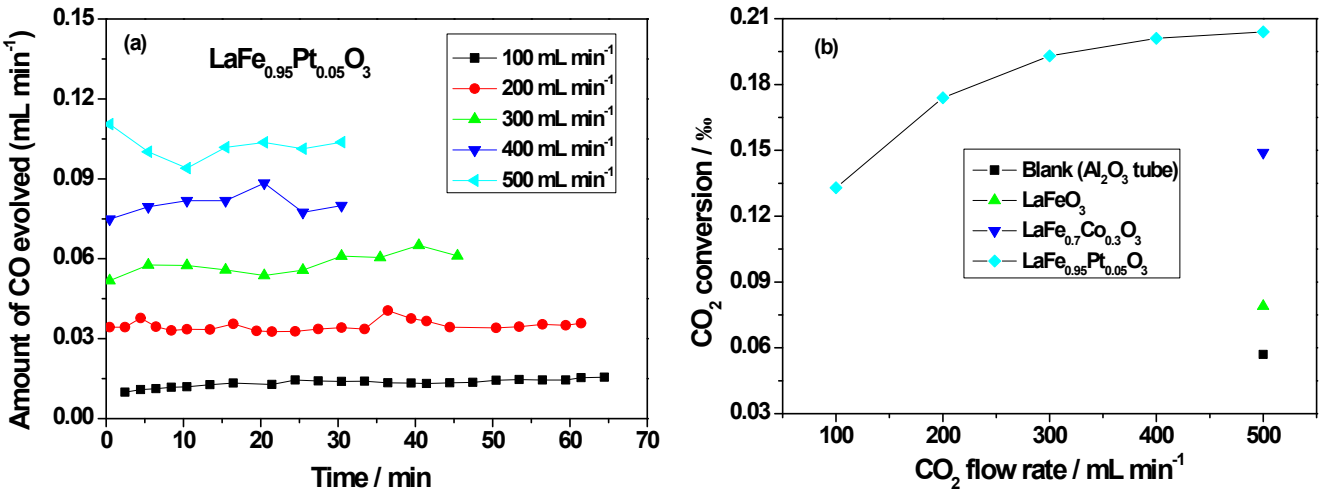

Figure S8. (a) The CO generation rate; (b) The CO_2 conversion ratio of $LaFe_{0.95}Pt_{0.05}O_3$ as a function of different CO_2 flow rate in direct CO_2-splitting reaction at 1300 °C (the CO_2 conversion of blank Al_2O_3 tube test is provided as a comparison).

9. The influence of intergranular gas diffusion

In order to study the influence of gas diffusion inside the layer of particles, the amount of $LaFe_{0.7}Co_{0.3}O_3$ powder introduced into the crucible was controlled. Generally, the sample was loaded into an alumina crucible with an inside diameter of 11 mm during the direct thermochemical CO_2-splitting reaction. The CO generation rate as a function of the metal oxide weight in direct CO_2 splitting reaction at 1300 °C is shown in Figure S7. It can be seen that the CO generation rate is increased from 0.05 mL min^{-1} up to 0.08 mL min^{-1} as the amount of $LaFe_{0.7}Co_{0.3}O_3$ increasing from 0.2 g to 0.5 g. However, by further increasing the amount of $LaFe_{0.7}Co_{0.3}O_3$ to 1.0 g, the reaction activity decreases a lot, which definitely points out the effect of mass-transfer limitations in the crucible. In other words, if too much oxide is present in the crucible, the produced CO and O_2 can't quickly diffuse into gas phase and then reverse reaction occurs. This behavior shows that the direct thermolysis of CO_2 is correlated to the amount of loaded sample and the CO and O_2 release rates are controlled by intergranular gas-phase diffusion in the material layer.

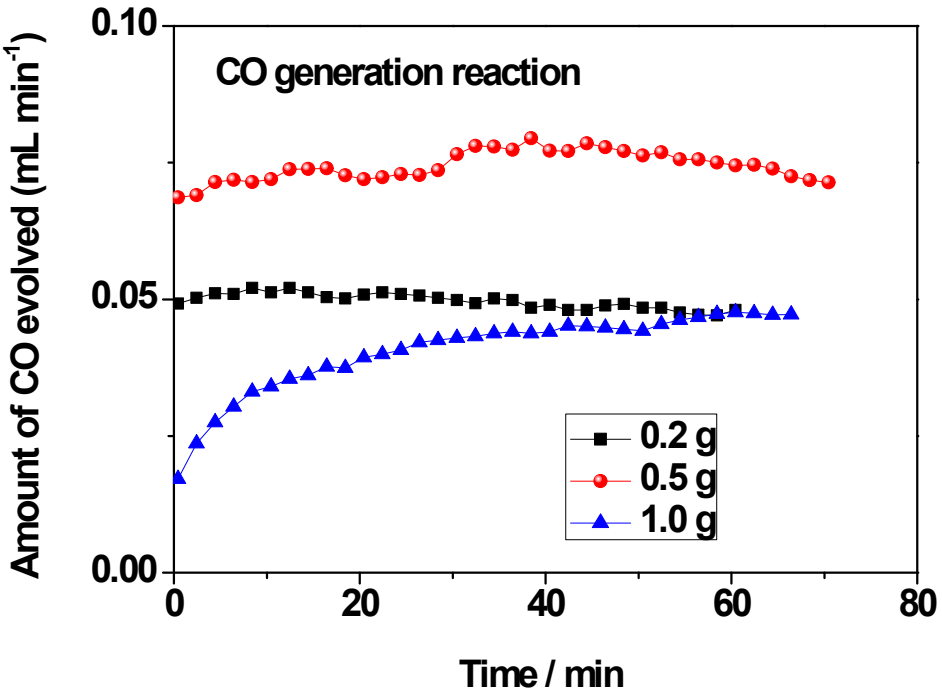

Figure S9. The CO generation rate of $LaFe_{0.7}Co_{0.3}O_3$ as a function of the weight of metal oxide in one-step CO_2-splitting reaction at 1300 °C.

10. The influence of pore structure of silica oxides

Silica oxides with different pore structure and different specific surface areas (SBA-15, MCM-41, commercial SiO_2) were also tested in direct CO_2 splitting reaction. The porous structure and large specific surface areas favors the CO_2 splitting rate obviously at first (Fig. R7) but the difference disappears gradually after longer reaction time.

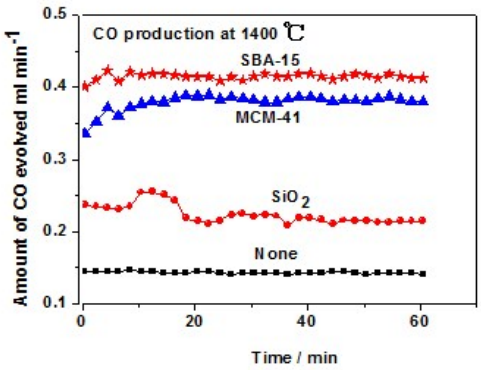

Figure S10. The CO_2 splitting rate with different silica oxides at 1400 ℃

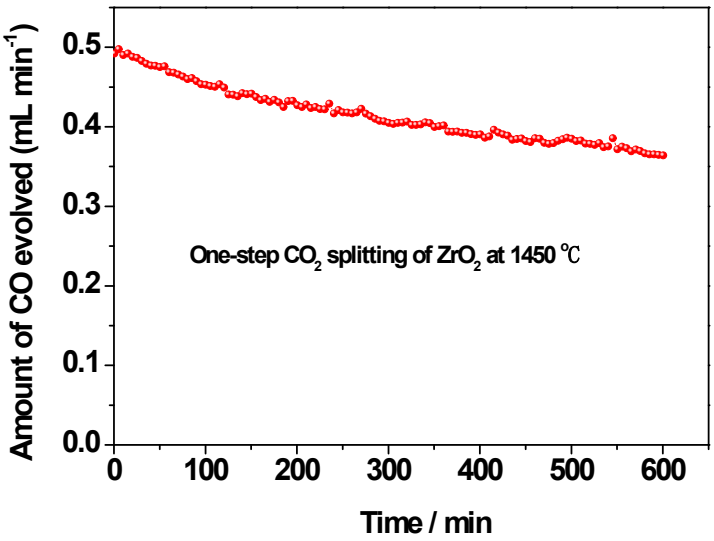

Figure S11. Stability test of the CO_2 thermolysis reaction in the presence of ZrO_2 at 1450 °C

REFERENCES

[1] a) J. L. Lyman, R. J. Jensen, *Sci. Total Environ.* **2001**, *277*, 7-14; b) A. J. Traynor, R. J. Jensen, *Ind. Eng. Chem. Res.* **2002**, *41*, 1935-1939; c) R. J. Price, D. A. Morse, S. L. Hardy, T. H. Fletcher, S. C. Hill, R. J. Jensen, *Ind. Eng. Chem. Res.* **2004**, *43*, 2446-2453.

[2] W. Tsang, R. F. Hampson, *J. Phys. Chem. Ref. Data* **1986**, *15*, 1087-1279.

[3] Q. Q. Jiang, Z. P. Chen, J. H. Tong, M. Yang, Z. X. Jiang, C. Li, *ACS Catal.* **2016**, *6*, 1172-1180.